Earth and Planetary Science Letters 297 (2010) 423–434

Contents lists available at ScienceDirect

Earth and Planetary Science Letters

journal homepage: www.elsevier.com/locate/epsl

Magnetotelluric deep soundings, gravity and geoid in the south São Francisco craton: Geophysical indicators of cratonic lithosphere rejuvenation and crustal underplating

Luis Gustavo Rodrigues Pinto [a,1], Marcelo Banik de Pádua [b], Naomi Ussami [a,*], Ícaro Vitorello [b], Antonio Lopes Padilha [b], Carla Braitenberg [c]

[a] Departamento de Geofísica, Instituto de Astronomia, Geofísica e Ciências Atmosféricas, Universidade de São Paulo, Rua do Matão 1226, 05508-090, São Paulo, Brazil
[b] Divisão de Geofísica Espacial, Instituto Nacional de Pesquisas Espaciais, Av. dos Astronautas 1758, 12227-010, São José dos Campos, Brazil
[c] Department of Earth Sciences, University of Trieste, Via Weiss 1, 34100 Trieste, Italy

ARTICLE INFO

Article history:
Received 10 June 2009
Received in revised form 15 June 2010
Accepted 24 June 2010
Available online 6 August 2010

Editor: L. Stixrude

Keywords:
cratonic lithosphere
rejuvenation
carbonatites
geoid
magnetotellurics
São Francisco craton

ABSTRACT

In the south São Francisco craton a circular and 8-m amplitude geoid anomaly coincides with the outcropping terrain of an Archean–Paleoproterozoic basement. Broadband magnetotelluric (MT) data inversions of two radial profiles within the positive geoid and Bouguer gravity anomaly yield geo-electrical crustal sections, whereby the lower crust is locally more conductive (10 to 100 Ωm) in spatial coincidence with a denser lower crust modeled by the gravity data. This anomalous lower crust may have resulted from magmatic underplating, associated with Mesoarchean and Proterozoic episodes of tholeiitic dike intrusion. Long-period MT soundings reveal a low electrical resistivity mantle (20 to 200 Ωm) from depths beyond 120 km. Forward geoid modeling, using the scope of the low electrical resistivity region within the mantle as a constraint, entails a density increase (40 to 50 kg/m^3) possibly due to Fe enrichment of mantle minerals. However, this factor alone does not explain the observed resistivity. A supplemented presence of small amounts of percolated carbonatite melting (~0.005 vol.%), dissolved water and enhanced oxygen fugacity within the peridotitic mantle are viable agents that could explain the less resistive upper mantle. We propose that metasomatic processes confined in the sub-continental lithospheric mantle foster the conditions for a low degree melting with variable CO_2, H_2O and Fe content. Even though the precise age of this metasomatism is unknown it might be older than the Early Cretaceous based on the evidence that a high-degree of melting in a lithospheric mantle impregnated with carbonatites originated the tholeiitic dike intrusions dispersed from the southeastern border of the São Francisco craton, during the onset of the lithosphere extension and break-up of the western Gondwana. The proxies are the NE Paraná and Espinhaço (130 Ma, Ar/Ar ages) tholeiitic dikes, which contain (~3%) carbonatites in their composition. The occurrence of a positive geoid anomaly (+10 m) and pre-tholeiites (age>138 Ma), carbonatites and kimberlites along the west African continental margin (Angola and Namibia) reinforces the presumed age of the São Francisco–Congo craton rejuvenation to be prior to its fragmentation in the Lower Cretaceous.

1. Introduction

Molina and Ussami (1999) have reported that the south São Francisco craton (SFC), in SE Brazil, is characterized by a positive, circular, 8-m amplitude residual geoid anomaly (Fig. 1), which coincides with the exposed Archean–Paleoproterozoic basement (Teixeira et al., 1996) limited by the meridional erosional front of the Neoproterozoic Bambui Group indicated as white dashed line in Fig. 2. The circular geoid positive anomaly has a diameter of approximately 500 km, centered at coordinates 44° W and 21° S over a broad topographic elevation ranging between 900 m and 1200 m above sea level and having the same wavelength. In the first attempt to interpret the SFC geoid high, Molina and Ussami (1999) obtained positive correlations of geoid and topography, which could not be explained by local (Airy or Pratt) isostatic models. The hypothesis of a thermal component within the lithosphere to support part of the topography was considered because of the proximity to the Vitoria–Trindade volcanic chain that extends eastward, at the same latitude, towards the Trindade hot spot. The lack of well-constrained crustal thickness information and reliable heat flow data hampered further investigation on the origin of this intracontinental geoid high.

Since this time, advances in geophysical studies carried out in SE Brazil during the 2000s contributed independent data, which have provided further insights on the origin of the SFC positive geoid anomaly. Upper mantle P- and S-wave tomography studies in SE Brazil (Schimmel et al., 2003; Feng et al., 2007) indicated that the south SFC lithosphere is characterized by positive velocity

* Corresponding author. Tel.: +55 11 30914787; fax: +55 11 30915034.
E-mail address: nussami@usp.br (N. Ussami).
[1] Presently at CPRM — Companhia de Pesquisa de Recursos Minerais, Rua Costa, 55, 01304-010, São Paulo, Brazil.

0012-821X/$ – see front matter © 2010 Elsevier B.V. All rights reserved.
doi:10.1016/j.epsl.2010.06.044

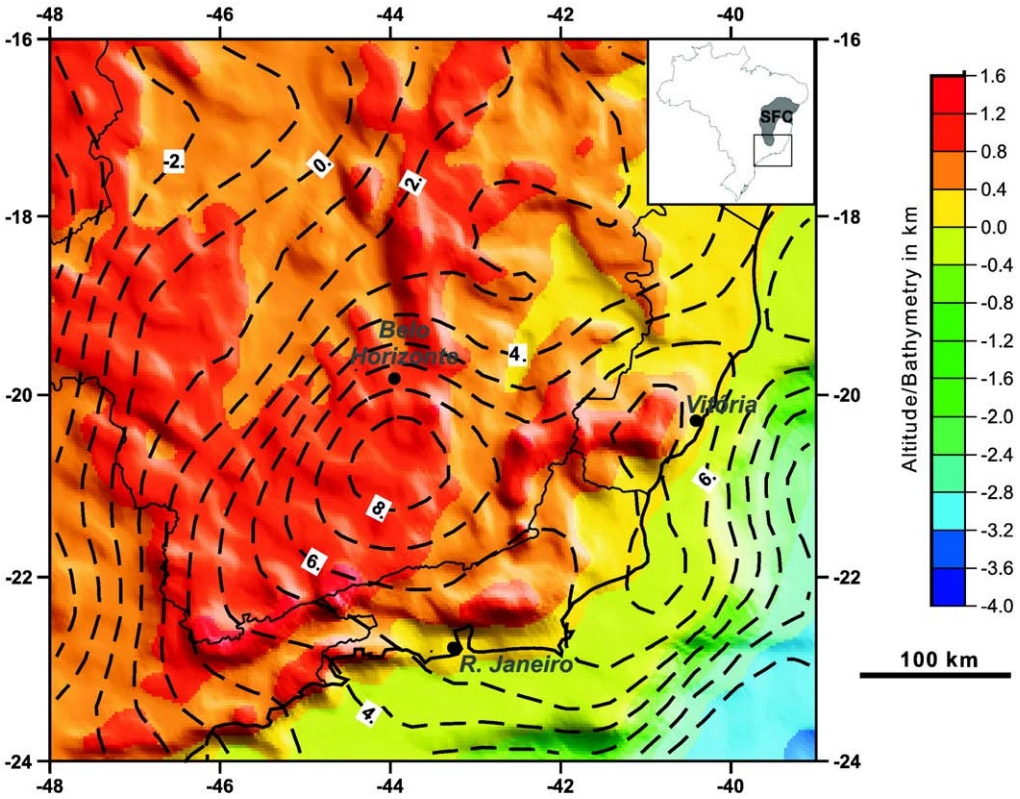

Fig. 1. Topography of the south SFC and bathymetry of the contiguous continental margin. Color scale at 400 m interval. Black dashed lines are 1-m contour interval of the geoid anomalies from Molina and Ussami (1999). Location of the study area shown in the inset map.

perturbations down to at least 200 km. Alexandrino and Hamza (2008) reported a highly variable range of heat flow (23 to 89 mW/m^2) for the region of the exposed basement in the southern SFC. A selection of eight sites, having the highest quality estimates, presents an average of 56.7 ± 20.5 mW/m^2. This result coincides with the global mean of 55 ± 17 mW/m^2, estimated by Pollack et al. (1993) for Proterozoic terrains, but it is in contrast with the mean of 41 ± 11 mW/m^2 for Archean cratons. Cratons are cold, very thick stable segments of continental lithosphere composed of ancient and chemically depleted mantle under a low lying topography. However, in recent years, geochemical studies of recurrent magmatism within cratons have shown that rejuvenation and underside erosion of cratonic lithospheres are more common than previously believed (e.g. Foley, 2008 and cited references within).

The present paper discusses new magnetotelluric (MT) deep sounding and gravity data, integrated with the previously identified geoid anomaly and recent geophysical and geological studies. It is proposed that the south SFC lithosphere underwent compositional changes as manifested by superficial magmatism, crustal underplating and refertilization of the lithospheric mantle subsequent to its consolidation at 1.8 Ga. A geophysical image of mantle metasomatism and rejuvenation of one segment of the former SFC–Congo cratonic lithosphere is depicted here for the first time.

2. Geological outline

According to Almeida et al. (1981), the SFC is the largest cratonic segment of the South American lithospheric plate. The core of the SFC remained isolated from tectonic processes younger than 1.8 Ga, except at its borders, during Pan-African/Brasiliano orogeny times (ca. 900 Ma) and its amalgamation into West Gondwana (Trompette, 1994). The proposed limits for the tectonically stable SFC by Alkmim et al. (1993) are those shown in Fig. 2 The exposed basement of the south SFC is limited to the north and west by the erosional front of the Bambui Group, a Neoproterozoic metasedimentary cover of the São Francisco basin, and to the south and east by the Late Neoproterozoic/Cambrian age Ribeira mobile belt (Machado et al., 1996).

Although the southern SFC is considered tectonically stable, it has experienced several magmatic episodes throughout its geological history as documented by the tholeiitic dike swarms starting in the Mesoarchean in the Bonfim Complex within the Quadrilatero Ferrifero region (QF in Fig. 2), the most abundant and thickest dikes within the SFC (Carneiro et al., 1998). According to Silva et al. (1995), the subsequent dike emplacement, at ca. 1.7 Ga, was related to the rifting phase of the Espinhaço basin formation. Younger magmatic episodes occurred at the eastern part of the SFC (ESP = Espinhaço dikes in Fig. 2) and according to Rosset et al. (2007) they are the Mesoproterozoic (~0.9–1.1 Ga) tholeiitic intrusions and the youngest magmatic episode, the high TiO_2 tholeiitic dikes of Early Cretaceous (ca. 130 Ma, $^{40}Ar/^{39}Ar$ ages). Early Cretaceous mafic dike swarms are also found in the Quadrilátero Ferrifero region (QF in Fig. 2, Silva et al., 1995; Pinese, 1997), along the Ribeira mobile belt (RMB in Fig. 2) and towards the continental margin (Guedes et al., 2005). Most of the Early Cretaceous tholeiitic magmatism is associated with the Western Gondwana break-up and the initial stages of the South Atlantic formation (Ernesto et al., 2002). The alkaline magmatism ranges from Late Cretaceous to Paleogene (Comin-Chiaramonti et al., 2007), within the sea floor spreading stage of the South Atlantic evolution. Along the southwestern margin of the SFC, kimberlites and kamafugites magmatism ages range from 120 Ma to 80 Ma, and the carbonatites magmatism is Late Early Cretaceous (Bizzi et al., 1995).

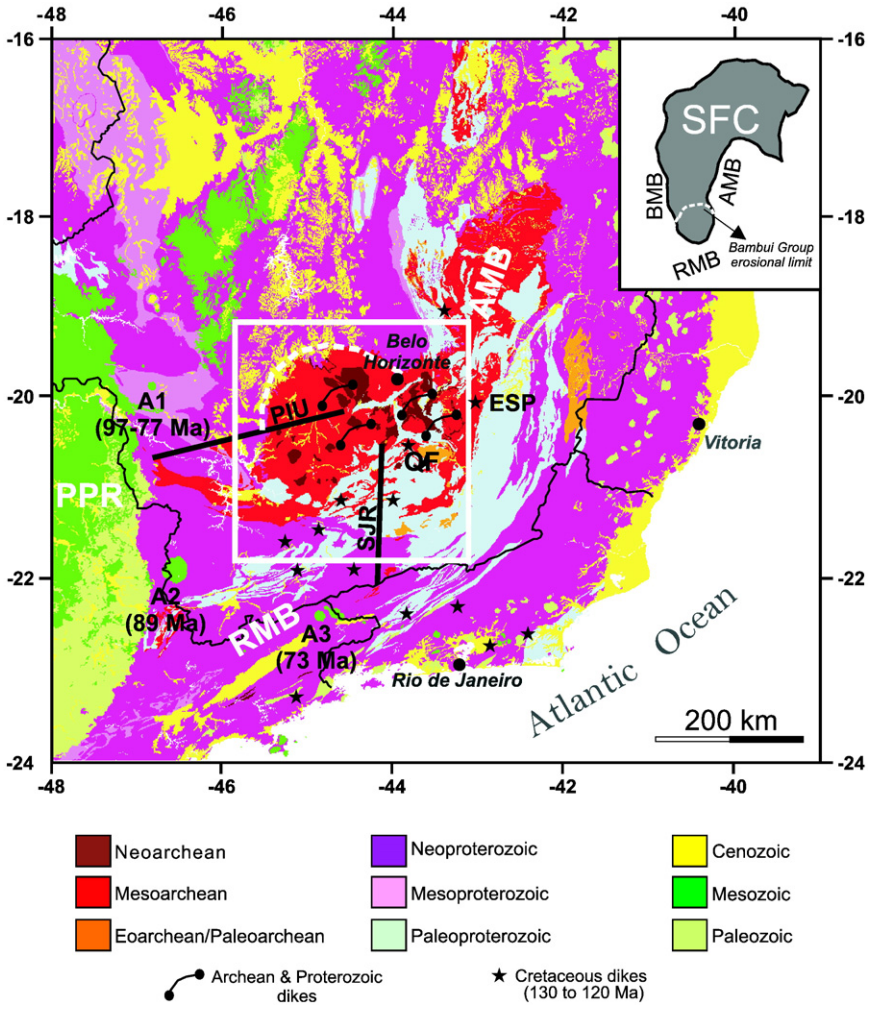

Fig. 2. Geological outline of the study area modified from Schobbenhaus et al. (2004). The inset figure shows the location of the study area, the limits of the entire SFC defined by the surrounding mobile belts, after Alkmim et al. (1993): BMB = Brasilia mobile belt, RMB = Ribeira mobile belt and AMB = Araçuai mobile belt. The dashed circular white line indicates the erosional boundary of the Neoproterozoic (~600 Ma) Bambui group. PPR = Paraná province; QF = Quadrilátero Ferrífero region; ESP = Espinhaço belt. PIU and SJR are the locations of the MT profiles. Upper Cretaceous alkaline/carbonatitic provinces are indicated as A1, A2, A3, with their respective ages in Ma.

3. Magnetotelluric (MT) deep soundings

3.1. Data acquisition

The MT method uses simultaneous measurements of natural time variations in the three components of the Earth's magnetic field (H_x, H_y, and H_z), and the orthogonal horizontal components of the induced electric field (E_x and E_y) to obtain the distribution of the electric conductivity in the Earth's interior. For this study, five electromagnetic components were recorded at each station and along two profiles, as shown in Fig. 2. The first profile is a 230-km long, ENE–WSW oriented profile named PIU and comprised of 16 stations. The second profile is a 160-km long, N–S oriented profile named SJR and comprised of 17 stations. Both profiles lie within the geoid anomaly high, as seen in Fig. 3.

MT soundings between 0.001 and 13,600 s were recorded to map the geo-electrical conductors within the crust and the lithospheric mantle. The soundings were carried out with two different MT systems, hereafter referred to as broadband and long-period equipment. The broadband MT systems collected data between 0.001 and 100 s, whereas the long-period soundings operated between 20 and 13,600 s. Thus, an overlap between the broadband and long-period soundings occurred from 20 to 100 s so that the results of each data acquisition procedure could be checked before composing a single sounding from 0.001 to 13,600 s at each station. Each profile was then composed of a complete sounding with data from both MT systems, alternating with a station made up of only the broadband sounding (Fig. 3).

Techniques for robust processing were applied to the data to yield MT and vertical field geomagnetic transfer function responses for each site (Egbert, 1997). A full description of the data acquisition and processing is given in Pádua (2004).

3.2. Groom–Bailey decomposition

The MT responses at each station were subsequently analyzed to correct for galvanic distortion effects caused by local near-surface local bodies, define the dimensionality of the data and to determine the most appropriate geo-electrical strike direction. The Groom–Bailey (GB) matrix decomposition technique (Groom and Bailey, 1989) was applied using the STRIKE program (McNeice and Jones, 2001). A single common strike value, which could be used for all stations in each one of the profiles, was estimated by fitting all of the measured impedance tensors. The strike values that gave the best fit were N25°W and N80°W for profiles PIU and SJR, respectively.

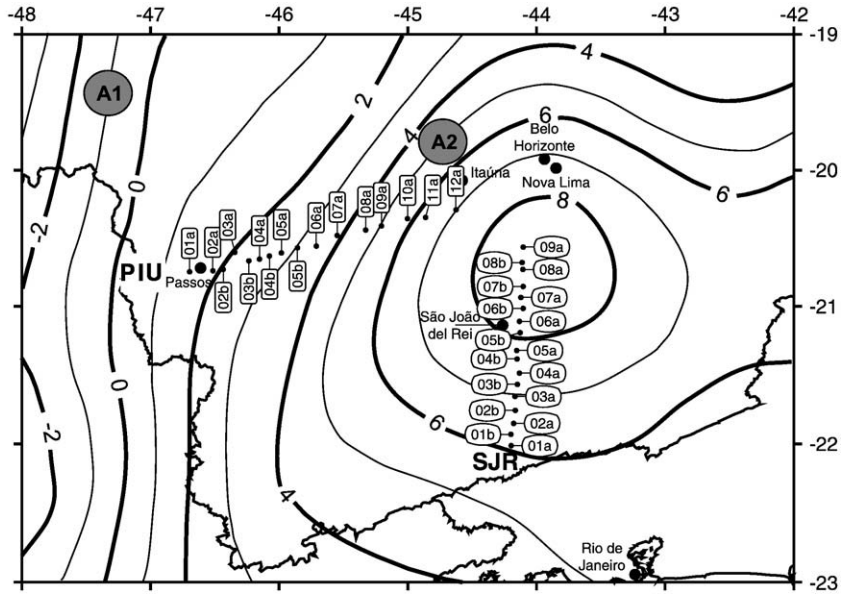

Fig. 3. Location of the two MT profiles together with their station numbers. The stations indicated by the letter a are stations with only broadband soundings, while the stations indicated by a letter b are those with both, broadband and long-period sounding MT systems. Contour lines are the residual geoid anomalies from Molina and Ussami (1999). Sites A1 and A2 are MT soundings carried out in other campaigns and discussed within the text.

3.3. MT data inversion

The PIU profile space model was comprised of 86 depth-columns, with each of the 78 central columns having a width of 3 km. The remaining eight lateral columns had the same width, with four columns set on each side of the profiles to avoid the edge effect within the 234-km long central part of the registered data. Along the vertical direction, the model space was similarly comprised of 39 layers with increasing thicknesses down to a depth of 200 km.

For the SJR profile, the same PIU procedure was adopted, except that along the horizontal direction, 66 columns existed, with 58 columns composing the central part and 4 lateral columns added at each end of the profile, for 174-km long model section.

The algorithm used to perform data inversion was the REBOCC (Reduced Basis Occam) algorithm proposed by Siripunvaraporn and Egbert (2000). The 2-D, geo-electrical model for both profiles made use of all available data (tipper, TM and TE apparent resistivity and phase). Results for the PIU profile are shown in Fig. 4(a), with an rms of 2.5. For the SJR profile, the results are shown in Fig. 4(b), with an rms of 2.97. In both cases the Lagrange multiplier, $\lambda = 100$ provided the most stable solution.

There are common lithospheric geo-electrical properties along the PIU and SJR sections shown in Fig. 4. The upper crust, from the surface to a depth of 20 km, is highly resistive, with values between $1000 < \rho < 100{,}000\ \Omega m$, as expected for anhydrous metamorphic rocks. In the SJR profile, the resistive upper crust is truncated by the localized, less resistive segments of the upper crust, which coincide with the mapped thrust faults of the Ribeira mobile belt (RMB), located in the southernmost end of the profile (see Fig. 2). In both sections, the mid- and lower-crust present low to intermediate resistivity ($10 < \rho < 500\ \Omega m$) in segmented regions. In the upper mantle, down to a depth of 200 km, a major lateral change in the geo-electrical property is observed for the southern

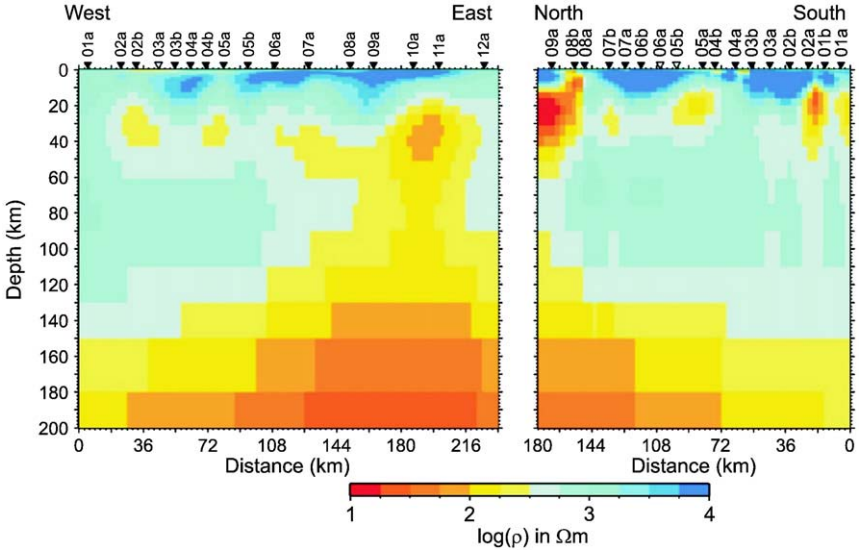

Fig. 4. Geo-electrical sections using the REBOCC inversion algorithm. (a) PIU profile (west–east) and (b) SJR profile (north–south), where both profiles cross one side of the geoid high.

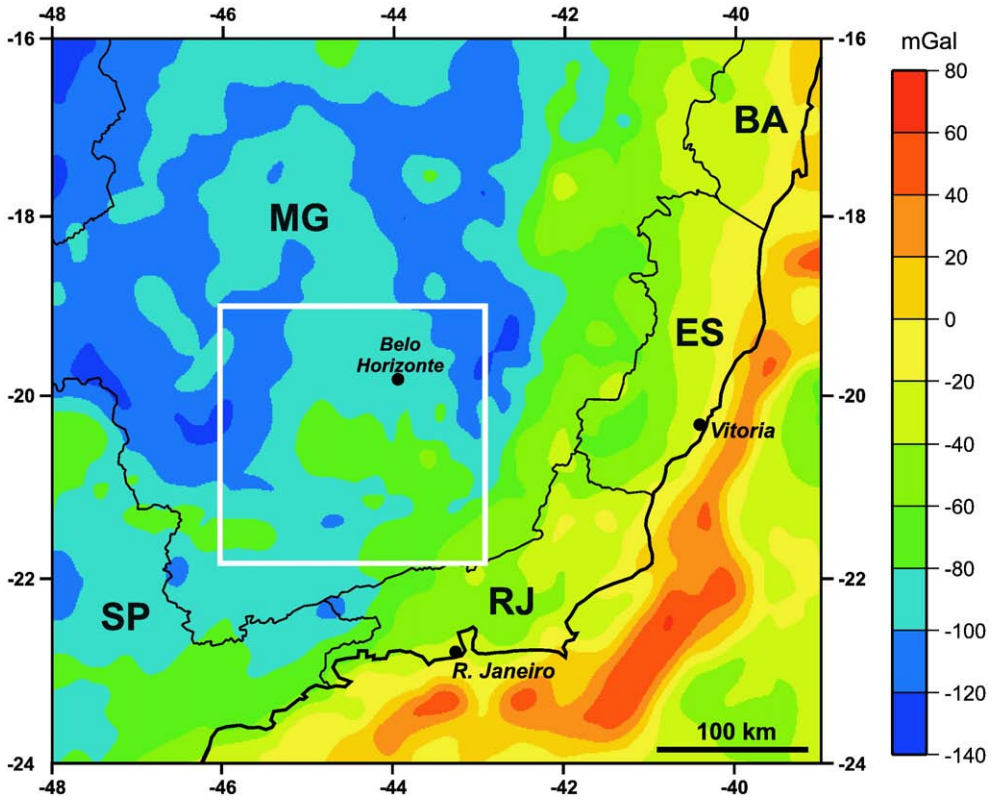

Fig. 5. Bouguer anomaly map of the study area. Color interval in mGal. The white square outlines the region where the residual gravity anomalies are shown in Fig. 6. The black lines are the state limits and the Atlantic coastline. The two letters symbols indicate the political states: SP = São Paulo, MG = Minas Gerais, RJ = Rio de Janeiro, ES = Espirito Santo and BA = Bahia.

SFC lithosphere and most clearly seen in the PIU section. The less resistive ($\rho < 100\ \Omega m$) mantle, below 120 km, extends upwards to shallower levels within the crust. This section defines a head-shaped high conductivity layer (10 to 500 Ωm), which spatially coincides, in plan view, with the geoid and Bouguer anomaly highs discussed in the following section.

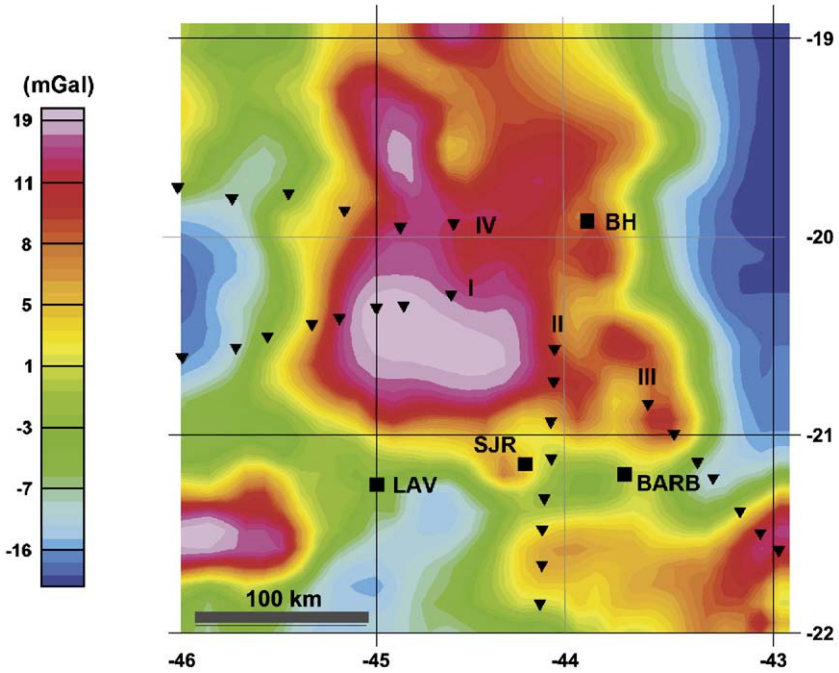

Fig. 6. Residual gravity anomalies within the region outlined by the white square in Fig. 5, after removal of a 3rd order polynomial regional field (Fig. 2S of Supplementary material). The locations of the MT profiles are indicated by Roman numerals: I and II are the MT profiles considered by the present study; III is the MT profile published by Figueiredo et al. (2008); and IV is the MT profile published by Bologna et al. (2007). Each MT station is indicated by a closed, inverted triangle. Cities are LAV = Lavras, SJR = São João del Rei, BARB = Barbacena, and BH = Belo Horizonte.

4. Gravity data

4.1. Bouguer anomaly data: regional and residual

The gravity data present a homogeneous distribution within the study area (see Fig. 1S map in the supplementary section), with approximately 12,000 gravity stations from the updated University of São Paulo data bank (Molina et al., 2000; Pinto et al., 2007), where each station is referenced to the International Gravity Standardization Network (IGSN) 1971. The Bouguer anomaly map, obtained after corrections for latitude using the 1967 Gravity Reference Formula and a density of 2670 kg/m^3 for Bouguer correction, is shown in Fig. 5.

The southern SFC residual gravity high is separated from the regional gravity field by using a third-order polynomial fitting (see Supplementary material Fig. 2S), and the results are shown in Fig. 6.

4.2. Residual gravity inversion

The first hypothesis to be tested was whether the source of the approximately 200-km wide positive residual anomaly shown in Fig. 6, covering mostly the Archean basement (Campo Belo and Bonfim complexes, Carneiro et al., 1998), could be caused by upper crust high density rocks. The crust of the SFC is composed of metamorphic rocks, with an average density of 2700 kg/m^3 (Ussami, 1986). If the positive anomaly was caused by higher density rocks within a 10-km layer in the upper crust, the local metamorphic Archean–Paleoproterozoic basement rocks should have a density contrast of +80 kg/m^3, which would correspond to an upper crust entirely composed by cryptic mafic rocks. According to Carneiro et al. (1998), gneissic rocks dominate the basement of the southern SFC, with relatively minor occurrences of amphibolitic and ultramafic rocks. A few occurrences of dike swarms with different ages intruding into the metamorphic basement of the southern SFC are reported as previously described (Section 2), which altogether would not explain the positive gravity anomaly. An alternative hypothesis would be crustal thinning. According to seismological receiver function estimates (França and Assumpção, 2004), there is no significant crustal thickness variation that could account for the 25-mGal amplitude and positive Bouguer residual gravity in this segment of the SFC. The average crustal thickness is about 39–40 km. A deeper origin for the gravity anomaly is unlikely due to the wavelengths of the residual gravity anomalies involved, and the unrealistic density contrast within the upper mantle that would be necessary to fit the observations. Therefore, the source of this gravity high should be a denser lower crust, and the most likely candidate would be the underplating of basic rocks at the base and within the lower crust. This hypothesis is consistent with the widespread occurrence of at least three generations of dikes in southeastern SFC and an electric, less resistive lower crust, as shown in Fig. 4.

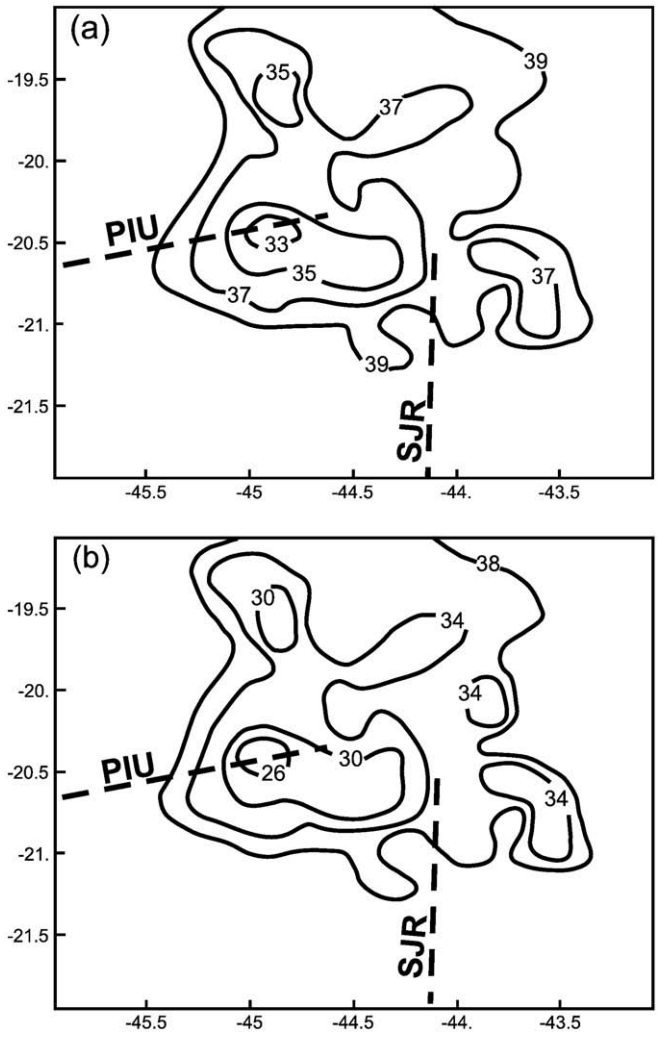

Fig. 7. Depth (in km) to a modeled denser lower crust intruded by mantle-derived material: (a) density contrast of 100 kg/m^3, (b) density contrast of 50 kg/m^3. The mean Moho depth was assigned at 40 km. The contour values indicate shallower depth to the top of the denser lower crust. The dotted lines are the location of MT profiles.

To model the higher density lower crust, we have assumed two density contrasts, 50 kg/m^3 and 100 kg/m^3, and a normal crust thickness of 40 km. The algorithm of Oldenburg (1974) was used to obtain the topography of the denser lower crust, which was found to vary from 22 to 33 km in depth depending on the value of density contrast or increase due to basaltic underplating as shown in Fig. 7a and b.

According to isostatic consideration (Watts, 2001, page 328), the underplated lower crust shown in Fig. 7a predicts an uplift of 1200 m, therefore consistent with present day local elevations which range between 900 m to 1000 m above sea level.

5. Geoid anomaly forward modeling

The results from the MT and gravity data inversion provide sturdy constraints to model the observed positive geoid anomaly. To forward model the observed geoid anomaly, we used a versatile formula to calculate the geoid effect due to a rectangular prism proposed by Nagy et al. (2000). Likewise, seismic tomography, which is sensitive to the elastic properties of the whole rock, along with the gravity and geoid anomalies, allowed us to map the bulk property of the rocks (density). The region within the crust and/or mantle of the anomalous density body may spatially coincide with the electrically anomalous region shown in Fig. 4, but they are not volumetrically or geometrically equivalent. In fact, electromagnetic methods, such as MT soundings, always depict a more diffuse distribution of the physical property, or the electrical conductivity, caused by some mineral phase present in the rock matrix.

To constrain the depth of the anomalous density region, the maximum depth rule proposed by Bowin et al. (1986), based on a point-mass formula to approximate the 3-D mass distribution, was initially used. The estimated maximum depth of the causative body from the observed geoid anomaly was 182 km and, therefore, located within the upper mantle. In Fig. 8, one possible density distribution solution is presented after forward modeling the observed geoid anomaly. The observed geoid anomaly was modeled using three prisms, one in the lower crust which represents the denser (+50 kg/m^3) underplating, and two prisms below the depth of 120 km, the top one with density contrast of +40 kg/m^3 and one at the bottom with a density increase of +50 kg/m^3.

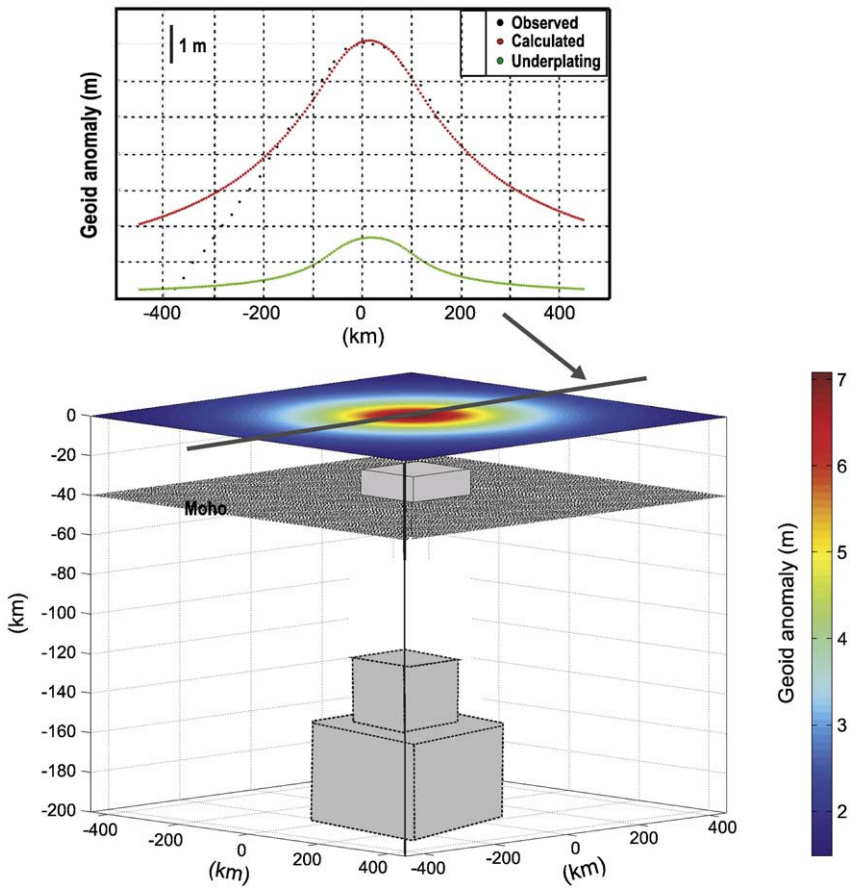

Fig. 8. Forward modeling of the geoid anomaly caused by prismatic bodies. Bottom and top prisms within the mantle with density contrasts of 50 and 40 kg/m^3, respectively, whereas the prism in the lower crust with density contrast of + 50 kg/m^3 is the underplating. The mean depth of the Moho is located at 40 km. The forward calculation was carried out using the Nagy et al. (2000) algorithm. The model assumes that below 200 km the density contrast vanishes.

Although this solution is not unique because different combinations of density contrasts and volumes of the prisms may produce the same observed geoid, the lateral extension of the density anomalous distribution is constrained by the geoid horizontal gradient and its vertical extension from the MT data, which mapped a lower electrical resistivity in the lower crust and below 120 km depth within the mantle. Additionally, the P-wave seismic tomography from Schimmel et al. (2003) and S-wave tomography by Feng et al. (2007) indicated that negative, Vp and Vs, velocity perturbations only occur below a depth of 200–300 km; therefore, according to seismic tomography, the bottom of this segment of the cratonic lithosphere persists at least to a depth of 200 km. A density reference value of 3400 kg/m^3 for anhydrous and electrically more resistive peridotite was assumed for the upper mantle. The assigned density contrasts (40 and 50 kg/m^3) for the modeling of the geoid anomaly corresponds to a density variation range between 1.0% and 1.5% relative to the assumed reference mantle density.

6. Discussion

Based on the results obtained from the MT soundings and the gravity modeling, we argue that the sources of the positive gravity and geoid anomalies are, respectively, a denser layer in the lower crust and a denser region spanning across the lithospheric mantle below, as summarized in Fig. 9. Additionally, the positive Bouguer gravity is probably related to crustal basaltic underplating, and the greater part of the positive geoid anomaly and the low electrical resistivity would be related to mantle refertilization by infiltrations of metasomatic agents, including iron, water and carbonatite components, within the peridotitic upper mantle from melts originating at depths below 180–200 km. We further discuss these points in the following sections.

6.1. Crustal low electrical resistivity and basaltic underplating

It has previously been demonstrated that the positive residual gravity anomaly is associated with a denser (~3–14 km thick) layer at the base and within the lower crust (Fig. 7). The density distribution at depths below the Moho, as inferred from the long-wavelength positive geoid anomaly, is not clearly depicted in the Bouguer gravity anomaly map because gravity is the first vertical derivative of the geoid anomaly. The positive density contrast in the lower crust contributes a shorter wavelength and a positive 2-m amplitude geoid anomaly. The most probable composition for this crustal layer is basaltic underplating based on the widespread occurrence of at least three generations of tholeiitic dike swarms (Carneiro et al., 1998). A less probable option would be eclogites derived from gabbros submitted to large pressures from intracratonic compressional events for which there is no evidence. An extensional tectonic regime is required to allow dike emplacement and this scenario is corroborated by the presence of a highly conductive layer in the lower crust. Similar relationship is observed in many places elsewhere (Jiracek et al., 1995). In an example from modern extensional regimes, highly conductive layers have been ascribed to electrolytic conduction provided by fluidized lower crust during basaltic underplating (Wannamaker et al., 2008). For paleo-events, as in our case, electronic conduction by highly conducting interconnected solid phases is more likely because it can endure succeeding deleterious processes and can also maintain a conductive network for a longer period.

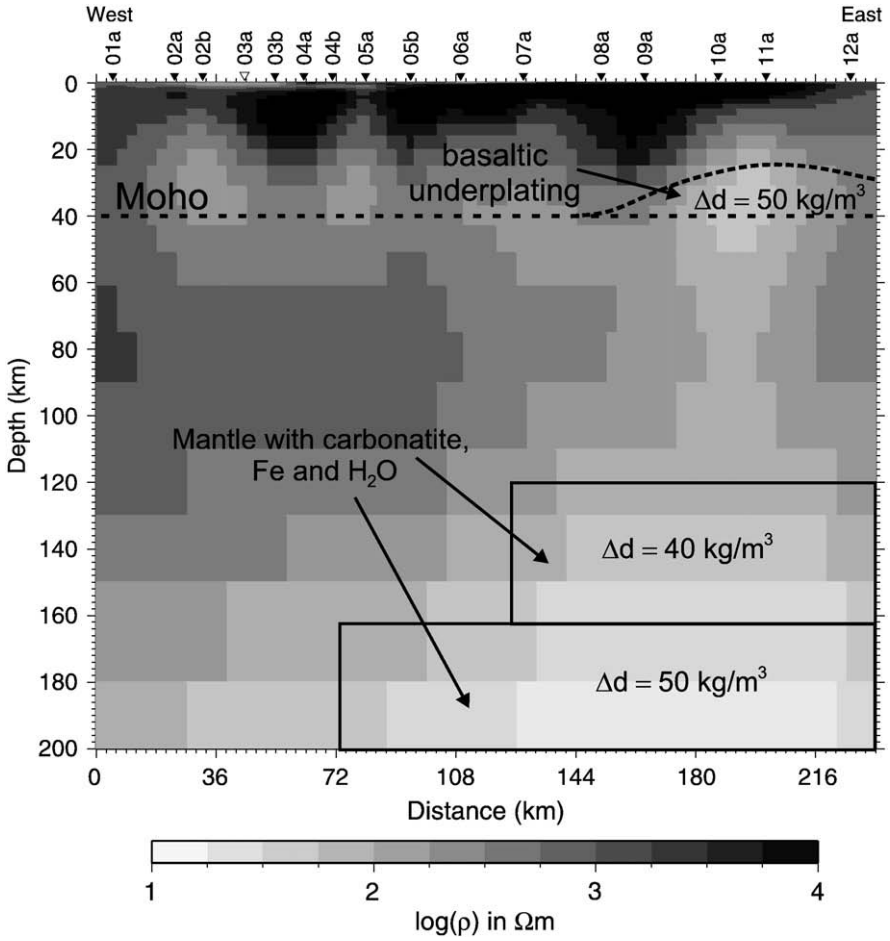

Fig. 9. Results of gravity inversion for the underplated lower crust with a density contrast of 50 kg/m^3 superimposed on the geo-electrical model obtained for the PIU profile. The horizontal black dashed line indicates the mean Moho depth estimated by seismic receiver function studies (França and Assumpção, 2004). A lithospheric mantle, at depths from 120 to 200 km, with resistivity lower than 300 Ωm, is considered as the main source of the positive geoid anomaly. Density contrasts increasing downward from 40 to 50 kg/m^3 are inferred to be associated with progressively denser metasomatic assemblages, possibly caused by a higher Fe content in the rejuvenated parts of the mantle.

The increased pressure found at depths below the brittle–ductile transition in the mid-lower crust can crunch porosity and permeability, thereby inhibiting conductivity by fluids. Additionally, retrograde metamorphism would consume free water at enhanced temperatures in the lower crust (Yardley and Valley, 1997). Therefore, we suggest that sulfides and graphitic film, a conducting phase believed to originate by precipitation from carbon-rich (CO_2 or CH_4) volatiles during the underplating event (Nover, 2005), to be responsible for the conductive layer in the SFC lower crust.

Fig. 9 shows the PIU geo-electrical section with its eastern portion crossing the central western segment of the positive residual gravity (Fig. 6). Fig. 9 also indicates the bulge (top at 22 km depth) of the proposed basalt underplate (Fig. 7b) that coincides with the region of high conductivity in the lower crust. The SJR geo-electrical section falls with its northern portion on the southwestern border of the positive residual gravity anomaly. It presents a very low resistivity layer (10 Ωm) below 20 km, in places where our proposed underplated lower crust reaches a depth of 33–34 km (Fig. 7b). The previously published MT section by Bologna et al. (2007), lying on the western side of the gravity high shown in Fig. 6, also presents a less resistive (100 Ωm) lower crust, at the site A2 shown in Fig. 3, the region consistent with the location of the modeled high density lower crust. The Figueiredo et al. (2008) MT study, with a profile (indicated with roman number III in Fig. 7) restricted over the Ribeira mobile belt, indicated upper crustal geo-electrical features that are similar to the SJR profile.

Fig. 10 is a synthesis of several depth-profiles of smooth-averaged resistivity values at selected MT sites in the study area. A wide range in the resistivity values of the crust and particularly the distinct values (10 to 100 Ωm) for the mid- and lower-crust resistivity for three sites (sjr09a, piu11a and A2) located within the positive residual gravity anomaly (Fig. 6) and for three sites (sjr02b, piu01a, A1) located outside the positive gravity anomaly, with resistivity above 1000 Ωm. Although no direct link in physical properties is expected between a denser basaltic underplating and enhanced conductivity, the deformations associated with the magma intrusion might have facilitated the infiltration of carbon- and metal-rich volatiles, coevally or not.

6.2. Low resistivity and density increase in the upper mantle

At mantle depths, both the PIU and SJR sections also present large variations in electrical properties. The regions that are more resistive occur along the sections outside the limits of the positive geoid. On the other hand, the portions of the geo-electrical sections that coincide with the circular positive geoid anomaly show highly conductive regions in the mantle, with an apparent shape similar to an upside-down funnel. As shown in Figs. 8 and 9, our proposed geoid model also involves a mass contrast in the mantle positioned approximately within the same low resistive encircled region.

To evaluate the effects of the various mechanisms that have been proposed to explain the enhanced conductivity at upper mantle depths (see Jones, 1999) we compare several resistivity depth-profiles (Fig. 10) with a resistivity depth-profile of nominally

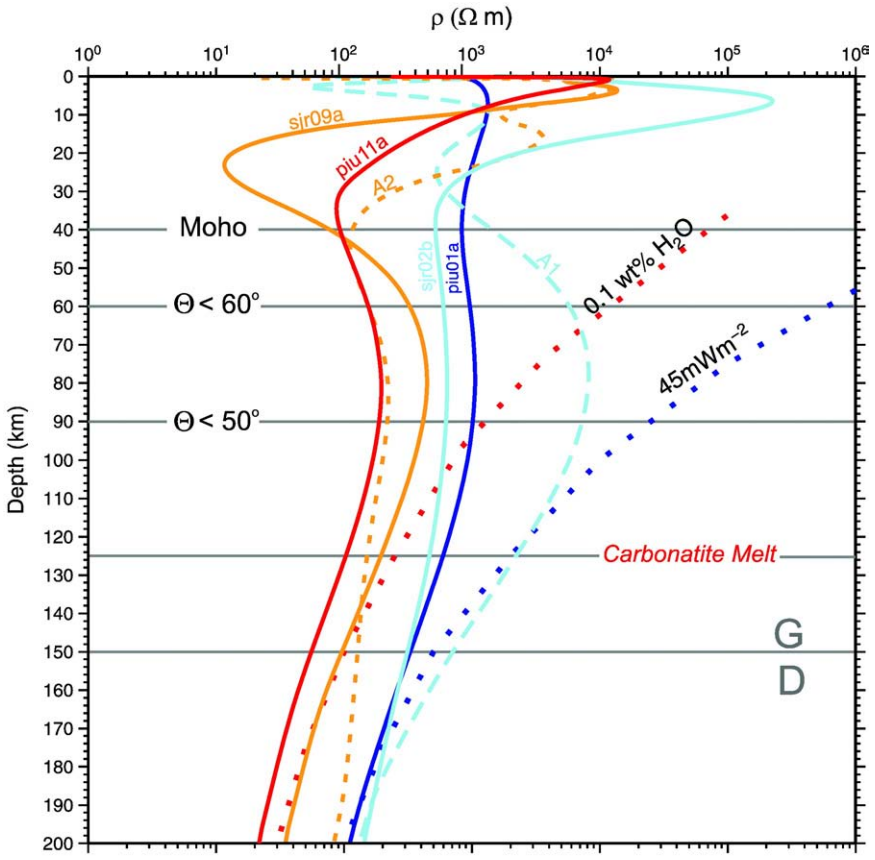

Fig. 10. Plot of resistivity versus depth-profiles of MT data from sites shown in Fig. 3, as colored continuous (sjr9a, piu11a, sjr02b and piu01a) and dashed (A1 and A2) lines. Resistivity depth-profiles of nominally anhydrous and hydrous (0.1 wt.% H_2O) upper mantle minerals for a 45 mW/m^2 reference geotherm, plotted as dotted blue and red lines, respectively. Depth indications for the Moho, dihedral angles, onset of carbonatite melting, and for graphite (G)–diamond (D) stability field transition.

anhydrous peridotite minerals obtained by transposing resistivity vs. temperature values from laboratory determinations (Yoshino et al., 2009) into a reference geotherm (Pollack and Chapman, 1977). Assuming a steady state conductive condition within a circular area of 500 km diameter, the resulting resistivity depth-profile for anhydrous upper mantle minerals represents the thermal component causing the attenuation of resistivity with depth for volatile-free peridotites. A resistivity depth-profile for anhydrous minerals, estimated with a 45 mW/m^2 geotherm, is fitted to a measured profile (A1) that presents the highest resistivity values in the region. The latter can be considered the upper bound geotherm of a typical resistivity profile of a volatile-free lithosphere beneath a stable craton, which is confirmed by the composition of xenoliths from several kimberlites in the study area, some of them diamondiferous (Pereira, 2007). Departures from this profile are assumed to be caused by non-thermal components. The large departures from the anhydrous profile observed at the uppermost mantle are partly derived from a smearing effect derived from the anomalous low resistivity that occurs in the lower crust by pulling down the measured resistivity immediately above and below the geo-electrical anomaly (Jones, 1999). Since the southern SFC is characterized by ultramafic magmatism (carbonatites, kimberlites, and kamafugites) that requires abundant metasomatic volatiles in the source mantle, we should consider the presence of pockets of fusible minerals, and enhanced water, carbon, iron and oxygen fugacity, which strongly affect the mantle rock electric conduction processes.

The effect of dissolved water can be evaluated from the resistivity profile estimated for undersaturated hydrous (0.1 wt.% H_2O) minerals (Yoshino et al., 2009) at temperatures related to a 45 mW/m^2 geotherm. However, regional MT responses over long periods indicate that the conductive structure in central-southeastern Brazil is only weakly anisotropic at the upper mantle depths (anisotropy factor around 3; Padilha et al., 2006), which is a typical result for a nominally dry lithospheric mantle (e.g., Du Frane et al., 2005).

In terms of iron enrichment, iron-rich mineral phases such as the rare fayalite and pyroxenite rocks in veins can present very low resistivities, but they probably occur in discrete and unconnected pockets. Nonetheless, even a plausible increment of the upper mantle bulk iron content from 10% to 20%, in accord with our geoid model, would decrease the resistivity of the most abundant anhydrous mantle minerals from ~400 Ωm to ~100 Ωm at 1227 °C (Vacher and Verhoeven, 2007), which corresponds to the ~150 km depth in Fig. 10. Yet, as reviewed by Jones et al. (2009), iron associated electrical conductivity enhancement in cratonic lithosphere is only of second order. The presence of interconnected graphite films in grain boundaries can provide low resistivity values only to its depth of equilibrium at ~150 km, defined by the assumed geotherm. However, at depths below 60 km the dihedral angle is probably larger than the critical angle of 60° (Mibe et al., 1998), and thus would inhibit an efficient fluid percolation of upwelling carbon-rich volatiles that would then precipitate in disconnected manners. Below these depths, the favorable dihedral angle and laboratory experiments indicate that the conductive phases that could explain the observed very low mantle electrical resistivity (~20 Ωm) are molten silicates or carbonates (Yoshino et al., 2006, Gaillard et al., 2008). In the study area, the assumed geotherm precludes the presence of partial silicate melts due to the anomalously high temperature or water content necessary for the onset of peridotite melting. Recent laboratory experiments (Gaillard et al., 2008) have shown that molten carbonates have electrical conductivities that could account for the

high conductivities seen in the asthenosphere below oceanic ridges. For the same amount of carbonate melts, the associated electrical conductivities are three or five orders of magnitude higher than for molten silicates or hydrated olivine, respectively. The presence of a small amount of carbonate melts (~0.005 vol.%) within peridotites would easily account for the observed electrical resistivity below 125 km in the southern part of the SFC. Moreover, if the high electrical conductivity of a large portion of the upper mantle is due to percolated carbonatites within a peridotite matrix, this result may also explain the presence of carbonatite (~3%) components in the Early Cretaceous Espinhaço tholeiitic dikes (see Fig. 16 of Rosset et al., 2007).

The next step would be to test whether the hypothesis of a small amount of carbonatite at depths greater than 125 km is consistent with independent geophysical data. To explain the geoid positive anomaly, we claim that, together with the impregnation of molten carbonates, a small amount of iron might have locally increased the mantle density by 50 kg/m^3. Seismic velocity should be affected by the presence of a molten phase and a density increase. Experiments carried out by Minarik and Watson (1995) demonstrated that carbonate melt remained interconnected to 0.05 wt.% melt in fine-grained olivine, which is a necessary condition to enhance the electrical conductivity and for molten carbonates to transport soluble and volatile elements within the mantle, including iron.

To evaluate whether the estimated density variation may be detected by S-wave tomography we start from the definition of S-wave velocity as $Vs = \sqrt{\frac{\mu}{d}}$, where μ is the rigidity modulus, and d is the density. To estimate the velocity perturbation ε_V due to a density variation ε_d, we derived the expression $\varepsilon_V = 0.5\, d^{-1} Vs\, \varepsilon_d$. Considering that the low estimated amount of carbonate melt does not affect the rigidity modulus, an upper bound for μ would be 10^{11} Pa. Assuming a reference mantle density of 3400 kg/m^3 and a surface velocity of 4.510 km/s between 150 and 200 km (Feng et al., 2007), the expected velocity reduction is 0.033 km/s for a density increase of 50 kg/m^3. This estimate is below the average rms misfit of 0.0975 km/s for the best S-wave velocity model of the upper mantle for South America (see Figs. 5 and 6 of Feng et al., 2007). However, the velocity perturbation estimated by these authors, which decreased from +7% at 100 km to +2% at 200 km, is consistent with a density increase from 40 to 50 kg/m^3 at the same depth interval in the south SFC mantle.

6.3. Age of lithosphere rejuvenation and metasomatism

The results presented above show compelling geophysical evidence of foregoing metasomatism, with carbonatite impregnating the upper mantle of the southern SFC lithosphere. The metasomatism that originated the higher density and lower electrical resistivity must have preceded the break-up of Gondwanaland because the Early Cretaceous tholeiitic dikes contain carbonatitic components (Rosset et al., 2007) derived from the high-degree melting of the rejuvenated upper mantle during lithospheric extension. However, on the Brazilian side of the former SFC–Congo craton (Trompette, 1994), occurrences of pre-tholeiites alkaline–carbonatite complexes were never reported either because they were never found, or because they existed but were eroded away or never intruded into this segment of the Archean–Proterozoic basement. On the contrary, in Angola and Namibia (or Congo craton), where the same positive geoid anomaly (+10-m amplitude) is observed (see Fig. 9 in Ernesto et al., 2002), several generations of Mesozoic to Cenozoic alkaline, carbonatites and kimberlites are preserved (Coltorti et al., 1993, Alberti et al., 1999, Comin-Chiaramonti et al., 2007). All of these authors attributed the carbonatites from Paraná–Angola–Namibia, as derived from the mantle heterogeneity resulting from metasomatic processes that occurred around 0.5–1.0 Ga. This metasomatism, apart from producing alkaline melts with variable CO_2 content, may have been accompanied by Fe enrichment to justify a denser mantle conduit associated with the geoid positive anomaly within the region of lower electrical resistivity. Angolan carbonatites show a compositional range from Ca- to Fe-carbonatites (Alberti et al., 1999), whereas Namibian carbonatites are mostly Fe- and rare Ca-carbonatites (Comin-Chiaramonti et al., 2007). Thompson et al. (2002) described an older magmatic event related to Ankerite ferrocarbonatite in Namibia, with a probable age of 1.1 Ga. According to Comin-Chiaramonti et al. (2007), the formerly depleted mantle comprising the Paraná–Angola–Namibia province was metasomatized at different times by small-volume melts, which formed veins (Foley, 1992, 2008) in a peridotite matrix. The time scale required for the asthenospheric-derived carbonatite melts to impregnate large areas in the lithosphere may be very short (100 to 1000 m in time scales of 0.1–1 My), as suggested by the laboratory experiments of Hammoud and Laporte (2000). Therefore, the suggestion that the carbonatitic rejuvenation event occurred prior to but very close to the West Gondwanaland break-up should be investigated further.

The role of the rejuvenation of a thick cratonic lithosphere in creating mechanical conditions ("zone of weakness") for the rupture of entire craton and the formation of new oceanic lithosphere has previously been suggested by Tappe et al. (2007) for the North Atlantic (NA) craton. Based on isotope geochemistry and precise dating of long-lived (~1200 My) alkaline and carbonatite magmatism on both sides of the Labrador sea margins, a history for the NA craton fragmentation was proposed that included successive melting phases, erosion and delamination of cratonic root and finally extension of a much thinner and weaker lithosphere. Seismic tomography of South America (Feng et al., 2007) and Africa (Priestley et al., 2008) indicated that the São Francisco and Congo cratonic lithospheres are at least 200 km thick, and according to paleomagnetic data they have remained as a single mass from the Mesoproteorozoic up to its break-up in the Mesozoic (Tohver et al., 2006). Geophysical and petrological data from the São Francisco–Congo craton suggest that this cratonic lithosphere has also undergone a long history of magmatic rejuvenation, which may provide an alternative explanation on how a 250-km thick cratonic lithosphere may rupture under plate tectonic forces (Buck, 2004). Carbonate melts, like any fluid, have wetting properties that may substantially modify the yield stress envelope of thick cratonic lithospheres (Michaut et al., 2009), reducing its total strength and making them more susceptible to fragmentation.

7. Conclusion

Broadband and long-period MT soundings, gravity and geoid modeling, integrated with previously published seismic tomography and heat flow data for the southern segment of the São Francisco craton have provided a physical image of a metasomatized upper mantle lithosphere. The use of MT soundings in tectonic settings, where regional scale geoid anomalies are observed, has proven to be effective in unveiling the geometry and important physical properties, such as the density and the electrical resistivity, of the crust and mantle, especially in a cratonic lithosphere affected by ensuing magmatic episodes. In the case of the south SFC, the mapped segment of the rejuvenated upper mantle, imaged by MT soundings and the modeling of the geoid anomaly, may have sensed an enriched, veined wedge within a peridotite matrix, amongst several other similar occurrences. These occurrences punctuate the sub-continental lithospheric mantle in SE Brazil and SW Africa, in addition to cratonic places where similar positive geoid anomalies are observed. Further investigation on the timing and the role of cratonic rejuvenation by carbonatitic melts along both margins may provide important constraints on the mechanisms by which the thick continental lithosphere broke apart and formed a new ocean.

Acknowledgements

To Enzo Piccirillo for discussion and insightful questions regarding Parana and South Atlantic magmatism, to Piero C. Chiaramonti for making us available his unpublished review on carbonatites and alkalines of S. America and Africa, to Nelsi C. de Sá for keeping the IAG-USP gravity data bank organized and available, and to Carlos Alberto M. Chaves for helping us in calculating the geoid effect. Suggestions from Garry Karner and one anonymous reviewer improved the original manuscript. This project was sponsored by FAPESP (Thematic Project 01/02848-0) and PhD scholarships to L.G.R. Pinto and M.B. Pádua. L.G.R. Pinto was also supported by a visiting PhD student (PDEE-CAPES grant) to Trieste University.

Appendix A. Supplementary data

Supplementary data associated with this article can be found, in the online version, at doi:10.1016/j.epsl.2010.06.044.

References

Alberti, A., Castorina, F., Censi, P., Comin-Chiaramonti, P., Gomes, C.B., 1999. Geochemical characteristics of Cretaceous carbonatites from Angola. J. Afr. Earth Sci. 29, 735–759.

Alexandrino, C.H., Hamza, V.M., 2008. Estimates of heat flow and heat production and a thermal model of the São Francisco craton. Int. J. Earth Sci. 97, 289–306.

Alkmim, F.F., Brito-Neves, B.B., Alves, J.A.C., 1993. Arcabouço tectônico do Cráton do São Francisco — uma revisão. In: Dominguez, J.L., Misi, A. (Eds.), O Cráton do São Francisco, Sociedade Brasileira de Geologia Núcleo Bahia/Sergipe, Salvador, pp. 45–62.

Almeida, F.F.M., Hasui, Y., Neves, B.B.B., Fuck, R.A., 1981. Brazilian structural provinces: an introduction. Earth Sci. Rev. 17, 1–29.

Bizzi, L.A., De Wit, M.J., Smith, C.B., Mc, Donald I., Armstrong, R.A., 1995. Heterogeneous enriched mantle materials and Dupal-type magmatism along the SW margin of the São Francisco Craton, Brazil. J. Geodyn. 20, 469–491.

Bologna, M.S., Vitorello, I., Padilha, A.L., Pádua, M.B., 2007. Restringindo propriedades físicas da litosfera no sul da província ígnea do Alto Paranaíba com dados magnetotelúricos: evidência de metassomatismo no manto. Extended abstracts of the Tenth International Congress of the Brazilian Geophysical Society, Rio de Janeiro, Brazil.

Bowin, C., Scheer, E., Smith, W., 1986. Depth estimates from ratios of gravity, geoid and gravity gradient anomalies. Geophysics 51, 123–136.

Buck, R.W., 2004. Consequences of asthenospheric variability on continental rifting. In: Karner, G.D., Taylor, B., Driscoll, N.W., Kohlstedt, D.L. (Eds.), Rheology and Deformation of the Lithosphere at Continental Margins. Columbia University Press, New York, pp. 1–30.

Carneiro, M.A., Carvalho Jr., I.M., Teixeira, W., 1998. Petrologia, geoquimica e geocronologia dos diques máficos do complexo metamórfico Bonfim Setentrional (Quadrilátero Ferrifero) e suas implicações na evolução crustal do Cráton do São Francisco Meridional. Rev. Bras. Geocienc. 28, 29–44.

Coltorti, M., Alberti, A., Beccaluva, L., Dossantos, A.B., Mazzuchelli, M., Morais, E., Rivalenti, G., Siena, F., 1993. The Tchivira–Bonga alkaline–carbonatite complex (Angola) — petrological study and comparison with some Brazilian analogs. Eur. J. Mineralog. 5, 1001–1024.

Comin-Chiaramonti, P., Gomes, C.B., Cundari, A., Castorina, F., Censi, P., 2007. A review of carbonatitic magmatism in the Parana–Angola–Namibia (PAN) system. Periodico Mineralog. 76, 25–78.

Du Frane, W.L., Roberts, J.J., Toffelmier, D.A., Tyburczy, J.A., 2005. Anisotropy of electrical conductivity in dry olivine. Geophys. Res. Lett. 32. doi:10.1029/2005GL023879.

Egbert, G.D., 1997. Robust multiple stations magnetotelluric data processing. Geophys. J. Int. 130, 475–496.

Ernesto, M., Marques, L.S., Piccirillo, E.M., Molina, E.C., Ussami, N., Comin-Chiaramonti, P., Bellieni, G., 2002. Paraná Magmatic Province–Tristan da Cunha plume system: fixed versus mobile plume, petrogenetic considerations and alternative heat sources. J. Volcanol. Geoth. Res. 118, 15–36.

Feng, M., Van der Lee, S.V., Assumpção, M., 2007. Upper mantle structure of South America from joint inversion of waveforms and fundamental mode group velocities of Rayleigh waves. J. Geophys. Res. 112. doi:10.1029/2006JB004449.

Figueiredo, I., Meju, M.A., Fontes, S.L., 2008. Heterogeneous crust and upper mantle across the SE Brazilian Highlands and the relationship to surface deformation as inferred from magnetotelluric imaging. J. Geophys. Res. 113 doi: p. 1/B03404-15.

Foley, S.F., 1992. Vein-plus-wall–rock melting mechanism in the lithosphere and the origin of potassic alkaline magmas. Lithos 28, 435–453.

Foley, S.F., 2008. Rejuvenation and erosion of the cratonic lithosphere. Nat. Geosci. 1, 503–510.

França, G.S., Assumpção, M., 2004. Crustal structure of the Ribeira fold belt, SE Brazil, derived from receiver functions. J. S. Am. Earth Sci. 6, 741–758.

Gaillard, F., Malki, M., Marziano, G.I., Pichavant, M., Scaillet, B., 2008. Carbonatite melts and electrical conductivity in the asthenosphere. Science 322, 1363–1364.

Groom, R.W., Bailey, R.C., 1989. Decomposition of magnetotelluric impedance tensor the presence of local three-dimensional galvanic distortions. Geophysics 56, 176–206.

Guedes, E., Heilbron, M., Vasconcelos, P.M., Valeriano, C.M., Almeida, H.C.H., Teixeira, W. Thomaz, Filho, A., 2005. K–Ar and $^{40}Ar/^{39}Ar$ ages of dikes emplaced in the onshore basement of the Santos Basin, Resende area, SE Brazil: implications for the south Atlantic opening and Tertiary reactivation. J. S. Am. Earth Sci. 18, 371–382.

Hammoud, T., Laporte, D., 2000. Ultrafast mantle impregnation by carbonatite melts. Geology 28, 283–285.

Jiracek, G.R., Haak, V., Olsen, K.H., 1995. Practical magnetotellurics in a continental rift environment. In: Olsen, K.H. (Ed.), Continental Rifts: Evolution, Structure and Tectonics. Elsevier, New York, pp. 103–129.

Jones, A.G., 1999. Imaging the continental upper mantle using electromagnetic methods. Lithos 48, 57–80.

Jones, A.G., Evans, R.L., Eaton, D.W., 2009. Velocity–conductivity relationships for mantle mineral assemblages in Archean cratonic lithosphere based on a review of laboratory data and Hashin–Shtrikman extremal bounds. Lithos 109, 131–143.

Machado, N., Valladares, C.S., Heilbron, M., Valeriano, C.M., 1996. U/Pb geochronology of Central Ribeira belt: implications for the evolution of Brasiliano orogeny. Precambrian Res. 79, 347–361.

McNeice, G.W., Jones, A.G., 2001. Multisite, multifrequency tensor decomposition of magnetotelluric data. Geophysics 66, 158–173.

Mibe, K., Fujii, T., Yasuda, A., 1998. Connectivity of aqueous fluid in the Earth's upper mantle. Geophys. Res. Lett. 25 (8), 1233–1236.

Michaut, C., Jaupart, C., Mareschal, J.C., 2009. Thermal evolution of cratonic roots. Lithos 109, 47–60.

Minarik, W.G., Watson, E.B., 1995. Interconnectivity of carbonate melt at low melt fraction. Earth Planet. Sci. Lett. 133, 423–437.

Molina, E.C., Ussami, N., 1999. The geoid in southern Brazil and adjacent regions: new constraints on density distribution and thermal state of the lithosphere. J. Geodyn. 28, 357–374.

Molina, E.C., Ussami, N., Marangoni, Y.R., 2000. Digital 5'×5' gravity maps of the São Francisco Craton, the marginal fold/thrust belts and contiguous continental margin/oceanic basins2nd ed. University of São Paulo, São Paulo. Explanatory text and CD-ROM.

Nagy, D., Papp, G., Benedek, J., 2000. The gravitational potential and its derivatives for the prism. J. Geodesy 74, 552–560.

Nover, G., 2005. Electrical properties of crustal and mantle rocks — a review of laboratory measurements and their explanation. Surv. Geophys. 26, 593–651.

Oldenburg, D.W., 1974. The inversion and interpretation of gravity anomalies. Geophysics 39, 526–536.

Padilha, A.L., Vitorello, I., Pádua, M.B., Bologna, M.S., 2006. Lithospheric and sublithospheric anisotropy beneath central-southeastern Brazil constrained by long period magnetotelluric data. Phys. Earth Planet. Inter. 158, 190–209.

Pádua, M.B., 2004. Estudo de indução eletromagnética na caracterização de estruturas profundas sob a borda sul do Cráton S. Francisco, Ph.D. Thesis, Instituto Nacional de Pesquisas Espaciais, São José dos Campos, 164 pp.

Pereira, R.S., 2007. Cráton do São Francisco, kimberlitos e diamantes. Ph.D. Thesis, Department of Geosciences, University of Brasilia, Brazil, 200 pp.

Pinese, J.P.P., 1997. Geoquímica, geologia isotópica e aspectos petrológicos dos diques máficos precambrianos da região de Lavras (MG), porção sul do Cráton do São Francisco, Ph.D. Thesis, Universidade de São Paulo, São Paulo, 178 pp.

Pinto, L.G.R., Ussami, N., Sá, N.C., 2007. Aquisição e interpretação de anomalias gravimétricas do Quadrilátero Ferrífero, SE do Cráton São Francisco. Rev. Bras. Geofísica 25, 21–30.

Pollack, H.N., Chapman, D.S., 1977. On the regional variation of the heat flow, geotherms, and lithospheric thickness. Tectonophysics 38, 279–296.

Pollack, H.N., Hurter, S.J., Johnson, J.R., 1993. Heat flow from the Earth's interior: analysis of the global data set. Rev. Geophys. 31, 267–280.

Priestley, K., McKenzie, D., Debayle, E., Pilidou, S., 2008. The African upper mantle and its relationship to tectonics and surface geology. Geophys. J. Int. 175, 1108–1126.

Rosset, A., De Min, A., Marques, L.S., Macambira, M.J.B., Ernesto, M., Renne, P.R., Piccirillo, E.M., 2007. Genesis and geodynamic significance of Mesoproterozoic and Early Cretaceous tholeiitic dyke swarms from the São Francisco craton (Brazil). J. S. Am. Earth Sci. 24, 69–92.

Schimmel, M., Assumpção, M., VanDeccar, J., 2003. Upper mantle seismic velocity structure beneath SE Brazil from P- and S-wave travel-time inversions. J. Geophys. Res. 108, 2191. doi:10.1029/2001JB000187.

Schobbenhaus, C., Gonçalves, J.H., Santos, J. O. S., Abram, M.B., Leão Neto, R., Matos, G.M.M., Vidotti, R.M., Ramos, M.A.B., Jesus, J.D.A., 2004. Carta Geológica do Brasil ao Milionésimo, Geographic Information System (GIS) and 46 sheets at 1:1.000.000 scale. CPRM-Companhia de Pesquisa de Recursos Minerais, Brasília. 41 CD-ROMS. ISBN: 85-7499-099-4.

Silva, A.M., Chemale Jr., F., Kuyumjian, R.M., Heaman, L., 1995. Mafic dike swarms of Quadrilátero Ferrifero and southern Espinhaço, Minas Gerais, Brazil. Rev. Bras. Geocienc. 25, 124–137.

Siripunvaraporn, W., Egbert, G.D., 2000. REBOCC: an efficient data-subspace inversion for two dimensional magnetotelluric data. Geophysics 65, 791–903.

Tappe, S., Foley, S.F., Stracke, A., Romer, R.L., Kjarsgarrd, B.A., Heamn, L.M., Joyce, N., 2007. Craton reactivation on the Labrador Sea margins: $^{40}Ar/^{39}Ar$ age and Sr–Nd–Hf–Pb isotope constraints from alkaline and carbonatite intrusives. Earth Planet. Sci. Lett. 256, 433–454.

Teixeira, W., Carneiro, M.A., Noce, C.M., Machado, N., Sato, K., Taylor, P.N., 1996. Pb, Sr and Nd isotope constraints on the Archaean evolution of gneissic–granitoid

complexes in the southern São Francisco craton, Brazil. Precambrian Res. 78, 151–164.
Thompson, R.N., Smith, P.M., Gibson, S.A., Mattey, D.P., Dickin, A.P., 2002. Ankerite carbonatite from Swartbooisdrif, Namibia: first evidence for magmatic ferrocarbonatite. Contrib. Mineralog. Petrol. 143, 377–395.
Tohver, E., D'Agrella Filho, M.S., Trindade, R.I.F., 2006. Paleomagnetic record of Africa and South America for the 1200–500 Ma interval and evaluation of the Gondwana assemblies. Precambrian Res. 147, 193–222.
Trompette, R., 1994. Geology of Western Gondwana (2000–500 Ma) Pan–African–Brasiliano: Aggregation of South America and Africa. A. A. Balkema, Rotterdam. 350 pp.
Ussami, N., 1986. Interpretation of Gravity Anomalies of Bahia state, Brazil. Ph.D thesis, University of Durham, 138 pp.
Vacher, P., Verhoeven, O., 2007. Modelling the electrical conductivity of iron-rich minerals for planetary applications. Planet. Space Sci. 55, 455–466.
Wannamaker, P.E., Hasterok, D.P., Johnston, J.M., Stodt, J.A., Hall, D.B., Sodergren, T.L., Pellerin, L., Maris, V., Doerner, W.M., Groenewold, K.A., Unsworth, M.J., 2008. Lithospheric dismemberment and magmatic processes of the Great Basin–Colorado Plateau transition, Utah, implied from magnetotellurics. Geochem. Geophys. Geosyst. 9. doi:10.1029/2007GC001886.
Watts, A.B., 2001. Isostasy and Flexure of the Lithosphere. Cambridge University Press. 458 pp.
Yardley, B.W.D., Valley, J.W., 1997. The petrologic case for a dry lower crust. J. Geophys. Res. 102, 12,173–12,185.
Yoshino, T., Matsuzaki, T., Yamashita, S., Katsura, T., 2006. Hydrous olivine unable to account for conductivity anomaly at the top of the asthenosphere. Nature 443. doi:10.1038/nature05223.
Yoshino, T., Matsuzaki, T., Shatsky, A., Katsura, T., 2009. The effect of water on the electrical conductivity of olivine aggregates and its implications for the electrical structure of the upper mantle. Earth Planet. Sci. Lett. 288, 291–300.